Materials Research Express

PAPER • OPEN ACCESS

Formation of EMT/FAU intergrowth and nanosized SOD zeolites from synthesis gel of zeolite NaX containing ethanol

Materials Research Express

PAPER

Formation of EMT/FAU intergrowth and nanosized SOD zeolites from synthesis gel of zeolite NaX containing ethanol

Nawee Jantarit[1], Pimwipa Tayraukham[1], Nattawut Osakoo[1,2], Karin Föttinger[3] and Jatuporn Wittayakun[1]

[1] School of Chemistry, Institute of Science, Suranaree University of Technology, Nakhon Ratchasima 30000, Thailand
[2] Institute of Research and Development, Suranaree University of Technology, Nakhon Ratchasima 30000, Thailand
[3] Institute of Materials Chemistry, Technische Universität Wien, Getreidemarkt 9, 1060 Vienna, Austria

E-mail: jatuporn@sut.ac.th

Keywords: zeolite NaX, EMT/FAU intergrowth, nanosized SOD zeolite, mesoporous zeolite, ethanol

OPEN ACCESS

RECEIVED
23 May 2020

REVISED
8 July 2020

ACCEPTED FOR PUBLICATION
13 July 2020

PUBLISHED
22 July 2020

Abstract

Ethanol can serve as an organic additive in zeolite synthesis due to the ease of availability and simple removal. It can influence the crystallization leading to zeolites with different phases and morphology. This study explores the effect of partial displacement of water in the synthesis gel of zeolite NaX by various amounts of ethanol. With one-pot synthesis, the gels with different ethanol/water molar ratios are crystallized 90 °C for 18 h under a static condition. The products are characterized by several techniques including X-ray diffraction (XRD), Fourier transform infrared spectroscopy (FTIR), scanning and transmission electron microscopy (SEM and TEM), nitrogen sorption analysis, inductively coupled plasma-optical emission spectrometry (ICP-OES), and thermogravimetric analysis (TGA). The ethanol/water molar ratio of 0.045 produces EMT/FAU intergrowth with a hollow structure and undefined shapes. The ratios of 0.412 and 0.628 give the aggregates of nanocrystalline SOD zeolite. Moreover, the molar ratios of 0.101, 0.174 and 0.273 provide a mixture of the three phases. All zeolite products contain both intrinsic micropores and interparticle mesopores. The higher ethanol/water molar ratio in the gel produces the zeolites with the lower Si/Al ratio due to the higher Al incorporation in the zeolite structure. In summary, we demonstrate alternative template-free approaches to synthesize EMT/FAU intergrowth and nanosized SOD zeolite with short crystallization time and low crystallization temperature. The finding is an example of ethanol influence on the crystallization to control the phase and morphology of zeolite.

1. Introduction

There are reports on the use of ethanol-containing gels in the synthesis of various zeolites, including ZSM-5 [1], mordenite [2, 3], zeolite Y [4], LTA [5] and sodalite [6, 7]. The presence of ethanol directly affects the gel properties such as density, pH, and concentration of sodium cation [6] that consequently influence the crystallization process. Ethanol could control morphology [1–7], or/and phase [5–7] of the zeolites. Huang *et al* [6] have reported that hollow nanosized sodalite with controllable size and morphology is synthesized from the gel of zeolite LTA with the ethanol-water system. Ethanol slows down the crystallization which affects the phase and particle size of the resulting zeolites. Moreover, ethanol accelerates the phase transformation of amorphous to sodalite. The results lead to a proposed mechanism of zeolite formation from a denser gel.

Zeolite X is a member of the FAU family with a Si/Al ratio in a range of 1.0–1.5. It is used as an absorbent and ion-exchanger due to its high ion-exchange capacity and large surface area [8]. Zeolite X can be synthesized by a template-free method under a mild condition [8]. However, the structure of zeolite X has high Al content, resulting in low thermal and hydrothermal stability [9]. The low stability implies that the gel of zeolite X could be easily transformed to other types of zeolite. There are reports that different phases are produced in the synthesis of the zeolite X, for example, LTA [10, 11], EMT/FAU intergrowth [12], SOD [13] and GIS [11, 14–16]. In this

Table 1. Amount of solvents in the gels and molar ratio of ethanol/water of all samples.

	Amount in the gel		
Sample	Water (g)	Ethanol (g)	Molar ratio of ethanol/water
E00	88.0	0.0	0.000
E10	78.0	10.0	0.045
E20	68.0	20.0	0.101
E30	58.0	30.0	0.174
E40	48.0	40.0	0.273
E50	38.0	50.0	0.412
E60	28.0	60.0	0.628

work, we report about the effect of ethanol in the gel of zeolite NaX on the formation to the transformation to other zeolite phases.

EMT/FAU intergrowth and nanosized SOD zeolites are the competitive phases of zeolite X. They are used as catalysts or supports for FCC gasoline hydro-upgrading [12], n-pentane hydroisomerization reaction [17], epoxidation reaction of 2-cyclohexan-1-one [18], Knoevenagel condensation [19]. The synthesis methods of EMT/FAU intergrowth suffer from the template requirement of site-directing agents such as 18-crown-6 or/and 15-crown-5 [12, 17], the long overall synthesis time and the complexity of crystallization method [20]. In the case of nanosized SOD zeolite, the synthesis requires a very high crystallization temperature [18, 19]. Consequently, the synthesis methods of EMT/FAU intergrowth and nanosized SOD zeolites have several drawbacks compared to the synthesis of zeolite X. The template requirement and high crystallization temperature could add up the cost to the synthesis.

Herein, we report the synthesis of EMT/FAU intergrowth and nanosized SOD zeolite by a template-free method from the ethanol-water system and low crystallization temperature. We explore the effect of ethanol on the phase, morphology, and porosity of the zeolites from the gel of zeolite NaX.

2. Experimental

2.1. Zeolite synthesis from ethanol-water system

The gels of zeolite X with the molar composition of $NaAlO_2$: $4SiO_2$: 16NaOH: $x H_2O$: yEtOH were prepared according to the literature [8]. The sample names, amounts of water, and ethanol corresponding to values x and y are shown in table 1. Sodium silicate solution (14.63 g) was obtained from mixing fumed silica (4.10 g, SiO_2, 99%, Carlo Erba), sodium hydroxide pellet (1.61 g, NaOH, analytical grade, Carlo Erba) and deionized water (8.92 g, DI) in a 250-ml polypropylene bottle under stirring for 18 h. Sodium aluminate solution (98.39 g) was prepared by adding sodium aluminate (1.36 g, anhydrous, Riedel-de Haën®) and sodium hydroxide pellet (9.08 g) into a solution (88.0 g) containing various amounts of DI water and ethanol (95%, commercial ethanol DEB95 (LC221200)) in another 250-ml polypropylene bottle under stirring for 1 h. Then, the solutions of sodium silicate and sodium aluminate were mixed and stirred for 1 h. The resulting gels were crystallized at 90 °C for 18 h under a static condition. The products were separated by centrifugation, washed with DI water, and dried at 110 °C for 24 h.

2.2. Sample characterization

The samples were analyzed by X-ray diffraction (XRD) patterns using Bruker D8 ADVANCE with Cu Kα radiation ($\lambda = 1.5418$ Å) operating with an increment of 0.02° at a scan rate of 0.2 s/step. The vibrational spectrum of zeolites was obtained by Fourier-transform infrared spectroscopy (FT-IR) on a Bruker Tensor 27 using Attenuated Total Reflectance (ATR) mode with a resolution of 4 cm^{-1} for 64 scans. N_2 adsorption-desorption analysis was conducted on Micromeritics ASAP 2020 at −196 °C (77 K). Before the analysis, each sample was degassed at 350 °C under vacuum. The specific surface area of the samples was calculated by Brunauer–Emmett–Teller (BET) method. The porous volume and pore size distribution were calculated by t-plot and Barrett–Joyner–Halenda (BJH) methods, respectively. Morphology and Si/Al ratio were analyzed by scanning electron microscopy (SEM) with energy-dispersive X-ray spectroscopy (EDS) using JEOL JSM 7800F field-emission scanning electron microscope (FE-SEM). The Si/Al ratio is also determined from inductively-coupled plasma- ICP-OES, Perkin Elmer Optima 8000). Each sample was digested in aqua regia, cooled down to room temperature, mixed with boric acid and DI water. The emission wavelength of silicon and aluminum in solid samples were detected at 251.611 and 396.153 nm, respectively, and compared with silicon tetrachloride

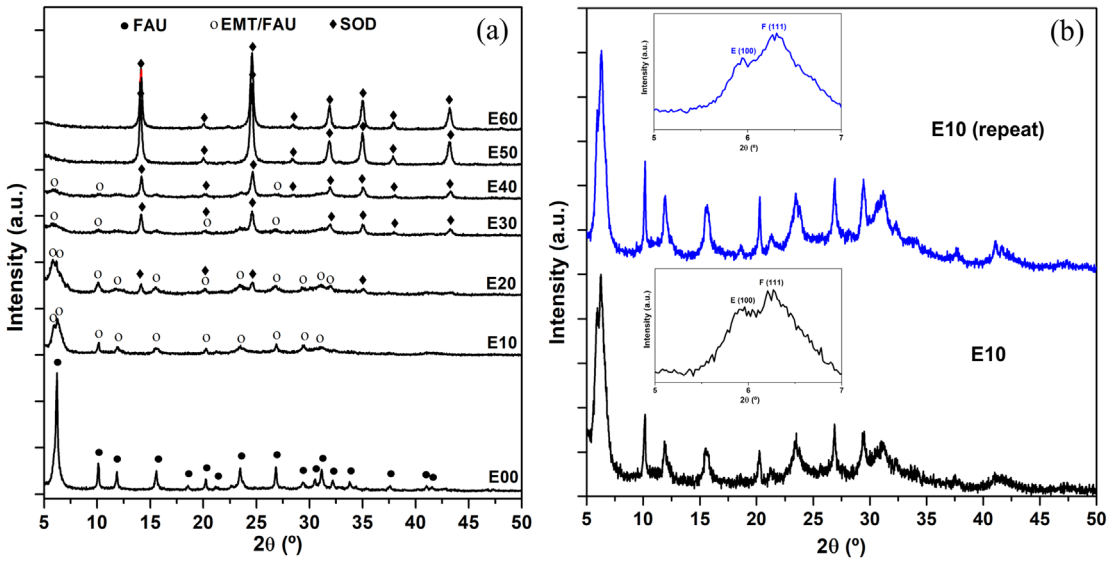

Figure 1. (a) XRD patterns of zeolites prepared from the synthesis gel of NaX with various amounts of ethanol, (b) comparison of the XRD patterns of the E10 from two syntheses.

and aluminum nitrate standards. Moreover, images from transmission electron microscopy (TEM) were from Thermo Scientific TALOS F200X operated at 200 kV. Thermal stability and weight loss of the samples were determined thermogravimetric analysis (TGA) and differential thermal analysis (DTA) using a Mettler Toledo model TGA/DSC1 in air with a flow rate of 50 ml min^{-1} at a heating rate of 10 °C min^{-1}. About 10.00 mg of the samples were placed in a pan prior to the analysis. Then, the curves of TGA and DTA were collected in the temperature in the range of 35 to 1000 °C.

3. Results and discussion

3.1. Phases of zeolite products from XRD

Figure 1(a) shows the XRD patterns of all samples crystallized from the synthesis gel of zeolite NaX with different ethanol/water molar ratios. The E00 sample is from the typical synthesis of the FAU-type zeolite X without ethanol addition. As expected, this sample shows only the characteristic peaks of FAU-type zeolite X [8].

The XRD pattern of the E10 sample shows peaks at positions similar to that of E00. However, the intensities are lower, indicating the lower crystallinity and smaller crystallite size. The first peak splits into two peaks at 5.9 and 6.2 degrees, meaning the false or twin stacking of the FAU layer in EMT/FAU intergrowth zeolite [21]. The low crystallinity and small crystallite size of the E10 sample is the result of ethanol content in the synthesis gel. Ethanol increases zeolite nucleation and slows down the crystallization process [6]. According to Gao *et al* [12], the higher sodium hydroxide in the synthesis gel of the FAU zeolite leads to the new phase formation, which could be a false or twin stacking of the FAU layer leading to EMT/FAU intergrowth. From the present work, the lower solubility of sodium hydroxide in ethanol leads to the higher sodium hydroxide concentration in the aqueous phase of the zeolite synthesis gel. To ensure that the synthesis of EMT/FAU intergrowth is reproducible, the synthesis was repeated with the same manners. The XRD pattern of E10(repeat) is compared with the first E10 in figure 1(b). The similar patterns confirm that the EMT/FAU intergrowth could be produced by the method in this present work.

From the literature, the EMT/FAU intergrowth has been synthesized from the gel with and without a template. With the template, the synthesis requires structure-directing agents such as 18-crown-6 or/and 15-crown-5, which ideally fit well with the sodalite cage layer of the hexagonal framework [22]. In the end, those reagents have to be removed by calcination. On the contrary, those agents are not necessary when ethanol is added as an additive to the synthesis gel. Since ethanol is easy to remove by evaporation, the calcination step is not required. Without template requirement, the EMT/FAU intergrowth was synthesized by the combination of two trajectories which has several steps and takes a long time to complete the crystallization [20]. The present work shows a one-pot method to synthesize the EMT/FAU intergrowth with shortening time and template-free. Thus, the new approach in the current work could reduce the synthesis cost, energy and time.

The XRD patterns of E20, E30, and E40 samples show a mixed phase of the EMT/FAU intergrowth and the SOD zeolite. With the more ethanol content, the gels become denser due to the higher Na_2O concentration and

Table 2. Si/Al ratios and, surface areas and pore volumes of all samples.

Sample	Si/Al ratio					
	ICP-OES	SEM-EDS	[a]S_{BET} (m^2 g^{-1})	[b]S_{Ext} (m^2 g^{-1})	[c]V_{Mes} (cm^3 g^{-1})	[d]V_{Micro} (cm^3 g^{-1})
E00	1.87 ± 0.03	1.45 ± 0.11	637	113	0.10	0.26
E10	1.87 ± 0.04	1.41 ± 0.08	507	130	0.18	0.19
E20	1.71 ± 0.05	1.30 ± 0.11	431	193	0.62	0.12
E30	2.05 ± 0.06	1.34 ± 0.00	170	93	0.41	0.04
E40	1.71 ± 0.03	1.33 ± 0.05	132	66	0.38	0.03
E50	1.71 ± 0.03	1.21 ± 0.05	44	33	0.28	0.01
E60	1.43 ± 0.02	1.26 ± 0.04	30	30	0.14	0.00

[a] specific surface area calculated by the BET method,
[b] external surface area,
[c] mesopore volume calculated by the BJH method,
[d] micropore volume calculated by the t-plot method.

pH in the aqueous phase. Such condition reduces the formation of the EMT/FAU intergrowth and favors the crystallization of SOD [6]. Finally, the XRD patterns of E50 and E60 samples exhibit only the characteristic peaks of the SOD zeolite with high intensity and sharpness. The larger ethanol content leads to the more concentrated gel which favors the crystallization of SOD zeolite.

There is a report on the effect of the decrease of water in the synthesis gel of zeolite X [23]. The results suggest that the synthesis with the less amount of water results in the smaller crystal size of zeolite X. No competitive phases of other zeolites are observed. In this work, the increase of ethanol/water molar ratio leads to the formation of the EMT/FAU intergrowth and SOD zeolite. So, one can conclude that the new phases are from the presence of ethanol. The formation of the SOD zeolite could be the result of the higher alkalinity in the denser gel due to the larger ethanol/water ratio. In the case of the formation of the EMT/FAU intergrowth, the ethanol molecule could coordinate with the specific crystal surfaces to prevent crystal growth [4]. This phenomenon might cause by the distortion of the FAU layer to create the EMT/FAU intergrowth.

3.2. Si/Al ratio of zeolite products determined by ICP-OES and SEM-EDS

The Si/Al ratio of the zeolite samples determined by ICP-OES and SEM-EDS are displayed in table 2. The ratio from ICP-OES represents the whole sample, whereas that from SEM-EDS reflects the surface composition. The different values from both techniques might be from the presence of the amorphous phase which normally has a higher Si/Al ratio [24]. The results show that the sample from the gel with a higher ethanol content tends to produce zeolite with a lower Si/Al ratio. Because the gel with higher ethanol content has less water and NaOH is less soluble in ethanol, the gel with the higher ethanol content has higher alkalinity. Thus, supersaturation of the synthesis gel is reached quickly leading to fast nucleation and more Al incorporation. This result is supported by the literature that the higher alkalinity of the synthesis gel prefers the Al incorporation in the zeolite framework [25, 26]. The Si/Al ratio of the E00 sample is in the range of FAU zeolite. The Si/Al ratios of the sample E10 from both techniques are more than those of EMT/FAU intergrowth in the literature [27] which may be from the presence of ethanol. Moreover, the Si/Al ratio of SOD (E50 and E60) in this work is higher than that in the literature [28].

3.3. Functional groups in zeolites from FTIR-ATR

Figure 2 shows the FTIR-ATR spectra of zeolite products with pure phase, namely, E00, E10, and E50. The vibrations of functional groups in the obtained samples are shown in table 3. The spectra of E00 and E10 are similar, indicating that FTIR cannot distinguish FAU zeolite and EMT/FAU intergrowth. This observation agrees with the work by Lohse *et al* [29] that FAU and EMT have similar FTIR spectra. However, all vibrational bands of E10 shift slightly to the lower wavenumber compared to those of E00, suggesting a lower Si/Al ratio in the skeletal structure of this sample [29]. These results are consistent with the Si/Al ratios from SEM/EDX and ICP-OES. The FTIR-ATR spectrum of E50 differs from those of E00 and E10. The intensity of the peak at 567 cm^{-1}, which corresponds to double-6-ring (D6R), is much lower due to the absence of D6R in the SOD structure.

Typically, FTIR-ATR is a surface analysis technique that distinguishes zeolite from amorphous silica. Vibration peaks of amorphous silica, particularly at 801 cm^{-1}, are not observed from the obtained zeolites. The results confirm that the zeolite surface does not contain amorphous silica. However, the high Si/Al ratio of the zeolite samples could be from the amorphous phase within the core of the particle [24].

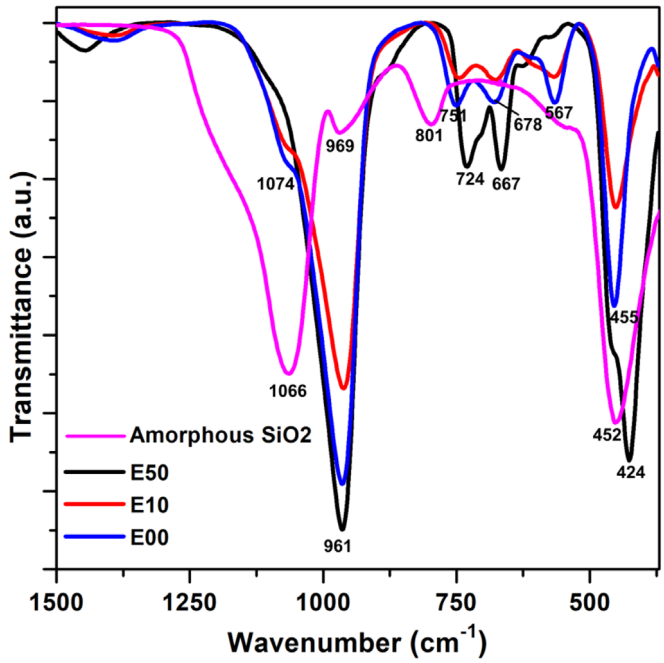

Figure 2. FTIR-ATR spectra in range of 400–1500 cm^{-1} of amorphous silica and the zeolite samples prepared with different ratios of ethanol/water.

Table 3. Band assignment and vibrational modes of amorphous silica, and FAU and SOD zeolites.

Wavenumber (cm^{-1})	Assignment	Reference
Species groups on FAU zeolite		[30]
455	Bending vibration of internal tetrahedral TO_4 (T = Si, Al)	
567	Vibration of double-6-ring (D6R)	
678 and 751	Symmetric vibrations of external linkage	
965	Asymmetric stretching vibration of Si–O–T bond	
1074	Vibration of Si-O bond in tetrahedral SiO_4	
SOD zeolite		[6]
424 and 460	Bending vibration of internal T–O–T	
667, 703 and 724	Symmetric stretching vibrations of T–O–T bond	
961	Asymmetric stretching vibration of T–O–T bond	
Amorphous silica		[31]
452	Bending vibration of Si–O–Si	
801 and 1066	Vibrations of Si–O bond	

3.4. Morphology from SEM and TEM

Figure 3 shows the SEM and TEM images of E00, E10, E50, and E60 samples, which are pure phase zeolites according to the XRD result. The E00 sample (figure 3(a)) consists of polycrystals with an average size of 1.4 μm. Each particle composes of nanosheets with an average thickness of 150 nm. The morphology is similar to NaX in our previous work [32].

The SEM image of the EMT/FAU intergrowth in E10 (figure 3(b)) shows the agglomerates with perforated hollow and undefined shapes. The morphology of small particles in the agglomerates (figure 3(c)) is house-of-card assemblies of the EMT/FAU nanosheets with an average size of 710 nm, which is similar to the morphology of EMT/FAU in the literature [20]. TEM image (figure 3(i)) shows the stacking faults of the sodalite layers in the EMT/FAU intergrowth, as shown in the red circle. This observation is similar to that of the EMT/FAU intergrowth prepared from the gel containing tetraethylammonium (TEA) [33]. The SEM images of E50 and E60 (figures 3(g) and (h)) show polycrystalline particles of nanosized SOD with the average diameters of 75 nm and 115 nm, respectively. A Higher ratio of ethanol/water in the gel provides a larger crystallite size of the SOD zeolite, which is consistent with the XRD result.

Moreover, the micrographs of the E20, E30 and E40 samples (figures 3(d)–(f)) show mixed morphology of polycrystalline particles with undefined shape, a typical morphology of the nanosized SOD zeolite [18], and the hollow shape which is similar to the morphology of the EMT/FAU intergrowth found in the E10. The amount of

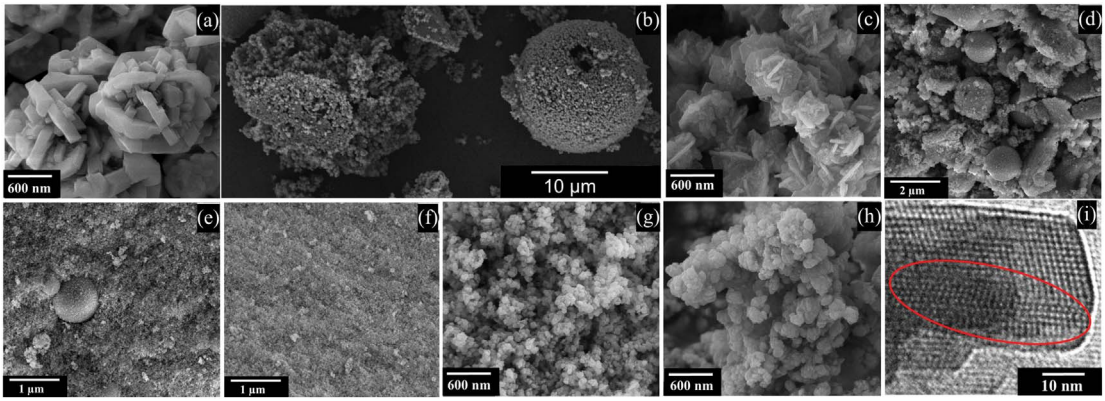

Figure 3. SEM images of the selected samples; (a) E00, (b) and (c) E10, (d) E20, (e) E30, (f) E40, (g) E50, (h) E60 and (i) bright-field mode with high-resolution TEM images of E10 showing the EMT-FAU intergrowth with the stacking fault of the EMT and FAU layers in a red oval area.

the hollow particles in the E20 sample is higher than that in the E30 while the amount of the polycrystalline particles in the E40 is higher than that of the E30 and the E20 samples which are consistent with the zeolite phases in the XRD patterns.

The results from XRD, SEM and TEM confirm that the zeolites from the synthesis gel with different ratio of ethanol/water have different phase and morphology. The zeolite formation in this work agrees with the reports from Huang *et al* and Möller *et al* [6, 34]. From the gel containing ethanol, denser gel agglomeration results in the formation of spherical particles. The spherical particle surface possibly serves as nucleation sites of zeolite. At the same time, numerous nuclei of the zeolite may grow quickly on the particle shell by consuming amorphous core as a nutrient to form the agglomeration of zeolite particles, which leads to the hollow structure of EMT/FAU intergrowth and polycrystal of nanosized SOD zeolite.

3.5. Results from N_2 adsorption-desorption analysis

Figures 4(a)–(c) shows the N_2 adsorption-desorption isotherms of all samples and figure 4(d) shows pore size distributions of samples with pure phase. The BET and external surface areas and pore volumes are listed in table 2. The adsorbed volume from E00 increases sharply at low pressure and becomes constant (figure 4(a)). This is the characteristic of type I(a) isotherm which is the adsorption in micropores of zeolite [35]. In the isotherm of E10, the adsorbed volume is lower than that of E00. This behavior could be attributed to the lower crystallinity of the EMT/FAU intergrowth. The isotherm also contains a hysteresis loop which indicates the presence of additional mesopore in this sample. The pore size distribution of E10 (figure 4(d)) exhibits an average size of 6.7 nm.

The isotherms of the E20, E30, and E40 samples (figure 4(b)) share the characteristic of the EMT/FAU intergrowth and the SOD zeolite. The SOD does not adsorb nitrogen because its pore size is smaller than the size of the nitrogen molecule. Thus, the decrease of FAU phase and the increase of SOD phase results in less adsorbed volume and, consequently, lower BET surface area. Moreover, the hysteresis loops at high pressure might be attributed to small aggregate particles of EMT/FAU and SOD zeolite [35, 36].

The isotherms of E50 and E60 (figure 4(c)) show very low adsorption at low pressure because these samples are pure SOD phase. The isotherms of these samples also consist of hysteresis loops at high pressure which is the behavior of nanosized zeolite [36]. The size of the hysteresis loop of E60 is smaller than that of E50 due to the larger crystal size. These results confirm that ethanol accelerates the crystallization of the SOD zeolite. From figure 4(d), both E50 and E60 samples show a broad pore size distribution in the range of mesopores but not in the same range as E10. E60 has less mesopore volume than E50 due to an increase of crystallinity, consistent with the XRD result. These results are consistent with the literature that the surface area nanosized SOD zeolite is higher than the micro-sized SOD zeolite [18].

3.6. Thermal decomposition of samples by TGA

Weight losses of the E00, E10, and E50 samples which are FAU, EMT/FAU, and SOD zeolites from thermogravimetric analysis are shown in figure 5(a). Their first derivatives are displayed in figure 5(b). The weight loss of E00 occurs continuously from the beginning to about 400 °C with the total loss of about 25%. Its DTA curve has a peak at 150 °C. The weight loss is due to loss of adsorbed waters on their surface, and in micro- and mesopores [37]. Compared to E00, E10 has similar TGA and DTA curves with smaller weight loss. The curve similarity suggests that the weight loss is from water. Moreover, these results imply that ethanol acts as the

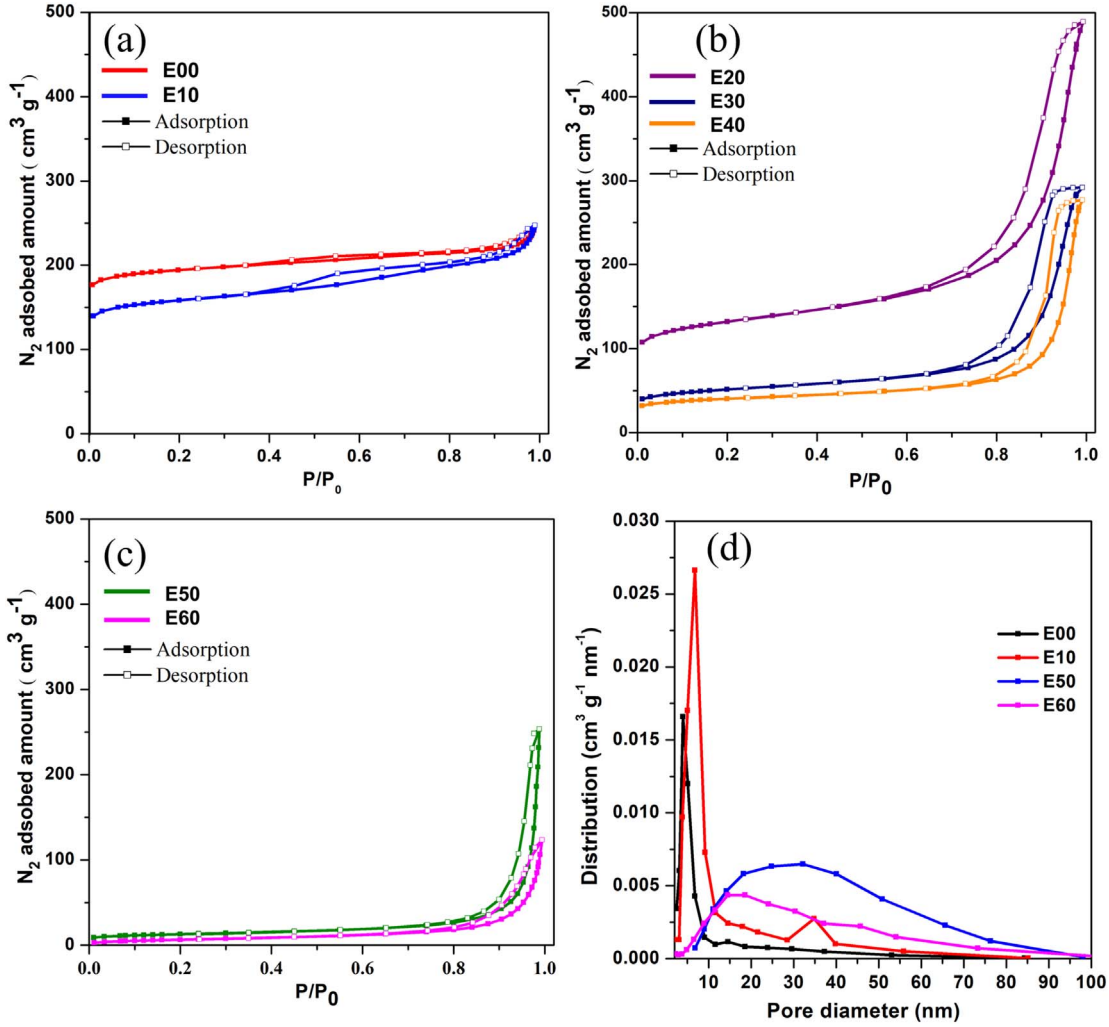

Figure 4. N_2 adsorption-desorption isotherms of (a) E00 and E10, (b) E20, E30 and E40, (c) E50 and E60, and (d) pore size distributions of E00, E10, E50, and E60.

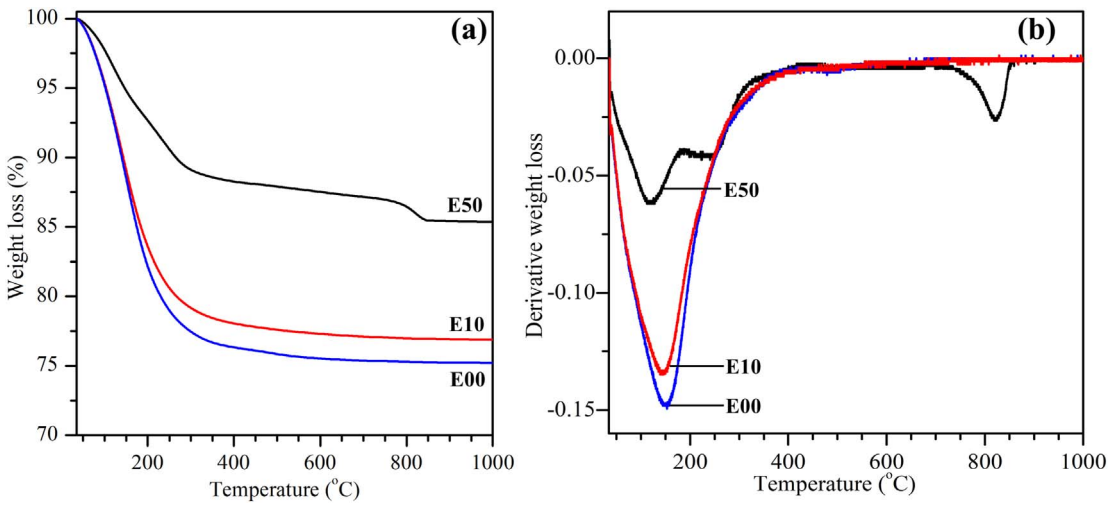

Figure 5. Thermogravimetric analysis of the synthesized samples including the E00 (blue line), E10 (red line), and E50 (black line) samples. Panel (a) TGA and (b) DTA curves.

organic additive, not an organic structuring agent. The less amount of water from E10 is consistent with the lower crystallinity and smaller surface area.

The TG and DTG curves of the E50 sample show three main peaks of weight losses. The two peaks around 120 and 250 °C are the loss of water molecules in ß-cage while the peak at 820 °C is caused by phase transformation of SOD zeolite to nepheline and/or α-carnegieite [38, 39]. Normally, SOD zeolite has a very low water adsorption capacity because the water molecules are not able to enter its small pores. However, the water adsorption capacity of nanosized SOD zeolite in this work is about 14.5%. This could be from the presence of additional mesopores.

The results from all techniques confirmed that nanosized SOD zeolite is obtained from the gel of zeolite NaX containing ethanol. Thus, this is an alternative method to synthesize nanosized SOD zeolite without template and low crystallization temperature.

4. Conclusions

We demonstrate that the EMT/FAU intergrowth and nanosized SOD zeolite can be produced by one-pot synthesis from the gel of zeolite NaX gel by tuning ethanol/water ratio. The ethanol/water ratio affects both final zeolite phases and morphologies. The higher ethanol/water ratio favors the crystallization of denser zeolite. The low ethanol/water ratio favors crystallization of the EMT/FAU intergrowth with hollow and undefined shapes. Moreover, polycrystals nanosized SOD zeolite is produced at the high ethanol/water ratio. Agglomeration of small or nanosized zeolite particles creates additional mesopores. The increase of ethanol/water ratio decreases the external surface area and mesopore due to larger zeolite particles of the SOD zeolite. High alkalinity resulting from the increase of ethanol/water ratio causes a high Al incorporation in zeolite structure resulting in the decrease of Si/Al ratio of the obtained zeolites.

Acknowledgments

N Jantarit is supported by the scholarship from the Thai government under the Development and Promotion of Science and Technology Talents (DPST) Project. P Tayruakham is supported by the Science Achievement Scholarship of Thailand (SAST). J Wittayakun acknowledges the scholarship Ernst Mach-Nachbetreuungsstipendium (EZA) through the Austrian Agency for International Cooperation in Education and Research (OeAD-GmbH). N Osakoo is supported by Full-Time Doctoral Researcher Grants from Suranaree University of Technology.

ORCID iDs

Jatuporn Wittayakun https://orcid.org/0000-0002-4426-2825

References

[1] Uguina M A, de Lucas A, Ruiz F and Serrano D P 1995 Synthesis of ZSM-5 from ethanol-containing systems. Influence of the gel composition *Ind. Eng. Chem. Res.* **34** 451–6
[2] Sano T, Wakabayashi S, Oumi Y and Uozumi T 2001 Synthesis of large mordenite crystals in the presence of aliphatic alcohol *Micropor Mesopor Mat.* **46** 67–74
[3] Oumi Y, Kakinaga Y, Kodaira T, Teranish T and Sano T 2003 Influences of aliphatic alcohols on crystallization of large mordenite crystals and their sorption properties *J. Mater. Chem.* **13** 181–5
[4] Chen Z, Chen C, Zhang J, Zheng G, Wang Y, Dong L, Qian W, Bai S and Hong M 2018 Zeolite Y microspheres with perpendicular mesochannels and metal@Y heterostructures for catalytic and SERS applications *J. Mater. Chem.* A **6** 6273–81
[5] Sharma P, Yeo J G, Yu J H, Han M H and Cho C H 2014 Effect of ethanol as an additive on the morphology and crystallinity of LTA zeolite *J. Taiwan Inst. Chem. Eng.* **45** 689–704
[6] Huang Y, Yao J, Zhang X, Kong C, Chen H, Liu D, Tsapatsis M, Hill M R, Hill A J and Wang H 2011 Role of ethanol in sodalite crystallization in an ethanol-Na_2O–Al_2O_3–SiO_2–H_2O system *CrystEngComm* **13** 4714–22
[7] Yao J, Zhang L and Wang H 2008 Synthesis of nanocrystalline sodalite with organic additives *Mater. Lett.* **62** 4028–30
[8] Mintova S and Barrier N 2016 *Verified Syntheses of Zeolitic Materials* 3rd ed. (Amsterdam: Elsevier (on behalf of the Synthesis Commission of the International Zeolite Association)) 978-0-692-68539-6
[9] Sadeghbeigi R 2012 *Fluid Catalytic Cracking Handbook* 3rd ed. (Oxford: Butterworth-Heinemann) 978-0-12-386965-4 (https://doi.org/10.1016/C2010-0-67291-9)
[10] Ansari M, Aroujalian A, Raisi A, Dabir B and Fathizadeh M 2014 Preparation and characterization of nano-NaX zeolite by microwave assisted hydrothermal method *Adv. Powder Technol.* **25** 722–7
[11] Maatoug N, Delahay G and Tounsi H 2017 Valorization of vitreous China waste to EMT/FAU, FAU and Na-P zeotype materials *Waste Manag.* **74** 267–78
[12] Gao D, Duan A, Zhang X, Zhao Z, Hong E, Qin Y and Xu C 2015 Synthesis of CoMo catalysts supported on EMT/FAU intergrowth zeolites with different morphologies and their hydro-upgrading performances for FCC gasoline *Chem. Eng. J.* **270** 176–86

[13] Hums E 2017 Synthesis of phase-pure zeolite sodalite from clear solution extracted from coal fly ash *J. Thermodyn. Catal.* **8** 1–6
[14] Musyoka N M, Petrik L F, Hums E, Kuhnt A and Schwieger W 2015 Thermal stability studies of zeolites A and X synthesized from South African coal fly ash *Res. Chem. Intermed.* **41** 575–82
[15] Hums E, Musyoka N M, Baser H, Inayat A and Schwieger W 2015 *In-situ* ultrasound study of the kinetics of formation of zeolites Na-A and Na-X from coal fly ash *Res. Chem. Intermed.* **41** 4311–26
[16] Dhainaut J, Daou T J, Chappaz A, Bats N, Harbuzaru B, Lapisardi G, Chaumeil H, Defoin A, Rouleau L and Patarin J 2013 Synthesis of FAU and EMT-type zeolites using structure-directing agents specifically designed by molecular modelling *Micropor Mesopor Mat.* **174** 117–25
[17] Belandría L N, Gonzàlez C S, Aguirre F, Sosa E, Uzcátegui A, González G, Brito J, González-Cortés S L and Imbert F E 2008 Synthesis, characterization of FAU/EMT intergrowths and its catalytic performance in n-pentane hydroisomerization reaction *J. Mol. Catal. A: Chem.* **281** 164–72
[18] Hiyoshi N 2012 Nanocrystalline sodalite: Preparation and application to epoxidation of 2-cyclohexen-1-one with hydrogen peroxide *Appl. Catal. A Gen.* **419–420** 164–9
[19] Shanbhag G V, Choi M, Kim J and Ryoo R 2009 Mesoporous sodalite: a novel, stable solid catalyst for base-catalyzed organic transformations *J. Catal.* **264** 88–92
[20] Gaber S, Gaber D, Ismail I, Alhassan S and Khaleel M 2019 Additive-free synthesis of house-of-card faujasite zeolite by utilizing aluminosilicate gel memory *Cryst. Eng. Comm.* **21** 1685–90
[21] Luo Y, Sun J, Zhao W, Yao J and Li Q 2002 Synthesis of zeolite EMT with aid of sodium phosphate *Chem. Mater.* **14** 1906–8
[22] Baerlochef C, Mccusker L B and Chiappettab R 1994 Location of the 18-crown-6 template in EMC-2 (EMT) Rietveld refinement of the calcined and as-synthesized forms *Micropor Mat.* **2** 269–80
[23] Ngoc D T, Pham T H and Nguyen K D H 2013 Synthesis, characterization and application of nanozeolite NaX from Vietnamese kaolin *Adv. Nat. Sci.: Nanosci. Nanotechnol.* **4** 1–12
[24] Cheong Y W, Wong K L, Ooi B S, Ling T C, Khoerunnisa F and Ng E P 2020 Effects of synthesis parameters on crystallization behavior of K-MER zeolite and its morphological properties on catalytic cyanoethylation reaction *Crystals* **10** 1–15
[25] Chatelain T, Patarin J, Brendlé E, Dougnier F, Guth J L and Schulz P 1997 Synthesis of high-silica FAU-, EMT-, RHO- and KFI-type zeolites in the presence of 18-crown-6 ether *Prog. Zeolite Microporous Mater.* ed H Chon, S K Ihm and Y S Uh 105 (Amsterdam: Elsevier Inc) 173–80
[26] Ferchiche S, Warzywoda J and Sacco A 2001 Direct synthesis of zeolite Y with large particle size *Int. J. Inorg. Mater.* **3** 773–80
[27] Khaleel M, Wagner A J, Mkhoyan K A and Tsapatsis M 2014 On the Rotational Intergrowth of Hierarchical FAU/EMT zeolites *Angew. Chemie Int. Ed.* **53** 9456–61
[28] Nanganoa L T, Mbadcam K J and Kang S 2016 Synthesis of hydroxy-sodalite from fine fractions of sandy clay loam soil (natural aluminosilicate) *Int. J. ChemTech Res.* **9** 725–32
[29] Lohse U, Pitsch I, Schreier E, Parlitz B and Schnabel K 1995 Cubic and hexagonal faujasites with varying Si/Al ratios I. Synthesis and characterization *Appl. Catal. A Gen.* **129** 189–202
[30] Zhou Y, Chen W, Wang P and Zhang Y 2018 EMT-type zeolite for deep purification of trace polar-oxygenated compounds from light olefins *Micropor Mesopor Mat.* **271** 273–83
[31] Tinio J V G, Simfroso K T, Peguit A D M V and Candidato R T 2015 Influence of OH^- ion concentration on the surface morphology of ZnO–SiO_2 nanostructure *J. Nanotechnol.* **2015** 1–7
[32] Rongchapo W, Keawkumay C, Osakoo N, Deekamwong K, Chanlek N, Prayoonpokarach S and Wittayskun J 2018 Comprehension of paraquat adsorption on faujasite zeolite X and Y in sodium form *Adsorpt. Sci. Technol.* **36** 684–93
[33] Delprato F, Delmotte L, Duth J L and Huve L 1990 Synthesis of new silica-rich cubic and hexagonal faujasites using crown-ether- based supramolecules as templates *Zeolites* **10** 546–52
[34] Möller K, Yilmaz B, Jacubinas R M, Müller U and Bein T 2011 One-step synthesis of hierarchical zeolite beta via network formation of uniform nanocrystals *J. Am. Chem. Soc.* **133** 5284–95
[35] Thommes M, Kaneko K, Neimark A V, Olivier J P, Rodriguez-Reinoso F, Rouquerol J and Sing K S W 2015 Physisorption of gases, with special reference to the evaluation of surface area and pore size distribution (IUPAC Technical Report) *Pure Appl. Chem.* **87** 1051–69
[36] Mintova S, Jaber M and Valtchev V 2015 Nanosized microporous crystals: emerging applications *Chem. Soc. Rev.* **44** 7207–33
[37] Ahmad H A, Bazin P, Fernandez C, Awala H and Mintova S 2016 Nanosized Na-EMT and Li-EMT zeolites: selective sorption of water and methanol studied by a combined IR and TG approach † *Phys. Chem. Chem. Phys.* **18** 30585–94
[38] Khajavi S, Sartipi S, Gascon J, Jansen J C and Kapteijn F 2010 Thermostability of hydroxy sodalite in view of membrane applications *Micropor Mesopor Mater.* **132** 510–7
[39] Fasolin S, Romano M, Boldrini S, Ferrario A, Fabrizio M, Armelao L and Barison S 2019 Single-step process to produce alumina supported hydroxy-sodalite zeolite membranes *J. Mater. Sci.* **54** 2049–58